

The signatures of the new particles h_2 and $Z_{\mu\tau}$ at e-p colliders in the $U(1)_{L_\mu-L_\tau}$ model

Jin-Xin Hou ^{*}, Chong-Xing Yue [†]

Department of Physics, Liaoning Normal University, Dalian 116029, China

Abstract

Considering the superior performances of the future e-p colliders, LHeC and FCC-eh, we discuss the feasibility of detecting the extra neutral scalar h_2 and the light gauge boson $Z_{\mu\tau}$, which are predicted by the $U(1)_{L_\mu-L_\tau}$ model. Taking into account the experimental constraints on the relevant free parameters, we consider all possible production channels of h_2 and $Z_{\mu\tau}$ at e-p colliders and further investigate their observability through the optimal channels in the case of the beam polarization $P(e^-) = -0.8$. We find that the signal significance above 5σ of h_2 as well as $Z_{\mu\tau}$ detecting can be achieved via $e^-p \rightarrow e^-j h_2(\rightarrow Z_{\mu\tau} Z_{\mu\tau}) \rightarrow e^-j + \cancel{E}_T$ process and a 5σ sensitivity of $Z_{\mu\tau}$ detecting can be gained via $e^-p \rightarrow e^-j h_1(\rightarrow Z_{\mu\tau} Z_{\mu\tau}) \rightarrow e^-j + \cancel{E}_T$ process at e-p colliders with appropriate parameter values and a designed integrated luminosity. However, the signals of h_2 decays into pair of SM particles are difficult to be detected.

I. Introduction

As is known, the standard model (SM) of particle physics is one of the most successful theories over the past decades which describes a variety of experimental results over the wide range of energy scale from eV to TeV. Discovery of the 125 GeV Higgs boson at the Large Hadron Collider (LHC) in 2012 [1, 2] proves the success of the SM once again. However, so far the SM still has certain limitations. Some experimental facts have been plaguing people, and there is an urgent need to extend the SM. For instance, the sub-eV masses and peculiar mixing pattern of neutrinos [3, 4], the muon $(g - 2)$ anomalous magnetic moment [5], the exploration of dark matter (DM) [6] and dark energy [7, 8], the baryon asymmetry of the Universe and so on. Furthermore, discovery of Higgs boson provides an outstanding portal to new physics (NP) beyond the SM. Precision measurements of the Higgs boson properties are also one of the most important tasks of high-energy particle physics due to its possible role as portal to beyond the SM (BSM) sectors [9–13].

So far, there are many well motivated extensions of the SM, such as SUSY [14–17], two Higgs doublet model [18–23], and extension of the SM with an extra $U(1)$ gauge group [24–30]. In this work, we will consider the gauged $U(1)_{L_\mu-L_\tau}$ extension of the SM due to its relatively simple theoretical structure, which has a complete gauge group $SU(3)_C \times SU(2)_L \times U(1)_Y \times U(1)_{L_\mu-L_\tau}$ and is called the $U(1)_{L_\mu-L_\tau}$ model [31–39]. One of the advantages of the $U(1)_{L_\mu-L_\tau}$ model is that the anomaly cancellation does not require any extra chiral fermionic degrees of freedom. In this model, the breaking of $L_\mu - L_\tau$ symmetry conduces to additional terms in the neutrino mass matrix, which offers an explanation for the neutrino

^{*}E-mail: houjinxin.email@yeah.net

[†]E-mail: cxyue@lnnu.edu.cn

masses and mixing simultaneously [37, 38]. Besides, the scalar sector has been expanded by two additional complex scalar singlets (φ_H and φ_{DM}) with nonzero $L_\mu - L_\tau$ charge. The scalar φ_{DM} can act as a viable DM candidate [40]. The other scalar φ_H acquires a vacuum expectation value (VEV) $v_{\mu\tau}$ and thereby making an additional neutral scalar h_2 after spontaneous breaking of $U(1)_{L_\mu-L_\tau}$, which indicates that h_2 has a mass of the same order with $v_{\mu\tau}$ about 10 GeV - 1000 GeV [36, 41]. In principle, the additional neutral scalar can be produced and decay via their mixing with the SM-like Higgs boson h_1 [51].

On the other hand, an extra neutral gauge boson $Z_{\mu\tau}$ is also introduced and obtains a mass after spontaneous symmetry breaking of $U(1)_{L_\mu-L_\tau}$. $Z_{\mu\tau}$ does not couple to the SM quarks and the first generation leptons, which makes it avoid restrictions coming from lepton and hadron colliders such as LEP and LHC. Therefore, the mass of $Z_{\mu\tau}$ can be as light as 100 MeV for a low value of gauge coupling $g_{\mu\tau} \leq 10^{-3}$, which is required to meet the limits arising from neutrino trident production. The $Z_{\mu\tau}$ with an MeV-scale mass can resolve the muon ($g-2$) anomaly, explain the deficit of cosmic neutrino flux [37, 43, 44] and resolve the problem of relic abundance of DM in the scenario with a light weakly interacting massive particle [45–47] simultaneously. Therefore, searching for its possible collider evidences plays a vital role in exploring NP. Many attempts to discover this kind of new particles have been made in the meson decay experiment [48], beam dump experiment [49], electron-positron collider experiments [50] and so on.

Searches for the new particles predicted by the $U(1)_{L_\mu-L_\tau}$ model are presently being conducted at the LHC and ILC [36]. While, another Higgs factory besides the LHC and ILC, such as the LHeC (Large Hadron electron Collider) and FCC-eh (Future Circular Collider in hadron-electron mode) [51–54], could precisely determine their specific properties. In this paper, we mainly devote to study of the h_2 and $Z_{\mu\tau}$ productions and further explore the possibility of detecting their signatures at e-p colliders. We present a full simulation study of the production cross sections of h_2 and $Z_{\mu\tau}$ with the beam polarization $P(e^-) = -0.8$. Then, we investigate their observability through the processes $e^-p \rightarrow e^-j h_2 (\rightarrow Z_{\mu\tau} Z_{\mu\tau}) \rightarrow e^-j + \cancel{E}_T$, $e^-p \rightarrow e^-j h_1 (\rightarrow Z_{\mu\tau} Z_{\mu\tau}) \rightarrow e^-j + \cancel{E}_T$ and $e^-p \rightarrow \nu j h_2 (\rightarrow ZZ) \rightarrow 2l^+ 2l^- j + \cancel{E}_T$, respectively. We further analyze the signal significance of h_2 and $Z_{\mu\tau}$ detecting which depends on the free parameters. Our numerical results show that the signals of $h_2 \rightarrow Z_{\mu\tau} Z_{\mu\tau}$ and $h_1 \rightarrow Z_{\mu\tau} Z_{\mu\tau}$ are promising to be detected at e-p colliders with appropriate parameter values and high integrated luminosity. But, due to the interference of substantial backgrounds and the low number of events, searching for the signal of the decay channel $h_2 \rightarrow ZZ$ are harder to achieve at e-p colliders.

Rest of the paper has been arranged in the following manner. In Sec. II, we briefly review the basic features of the $U(1)_{L_\mu-L_\tau}$ model and show the allowed parameter space of this model. In Sec. III, we not only give the partial widths of the main decay channels of the scalar h_2 , but also calculate its production cross sections via the W^+W^- and ZZ fusion processes. The production cross sections of the new gauge boson $Z_{\mu\tau}$ through h_2 and h_1 decays are calculated in Sec. IV. We estimate the numbers of the signal and background events, and investigate the signal observability and discovery potentiality of h_2 and $Z_{\mu\tau}$ through their respective promising production channels in Sec. V. Finally, our conclusions are given in Sec. VI.

II. The Basic Features of the $U(1)_{L_\mu-L_\tau}$ Model

The gauged $U(1)_{L_\mu-L_\tau}$ extension of the SM is one of the most extensively studied NP models, which can successfully solve the origin of tiny neutrino masses, the DM relic abundance and the muon $(g-2)$ anomalous magnetic moment. Refs. [37,38] have made a detailed analysis about solving these puzzles in the $U(1)_{L_\mu-L_\tau}$ model. In this model, the gauge sector of the SM is enhanced by imposing a local $U(1)_{L_\mu-L_\tau}$ symmetry to the SM Lagrangian, where L_μ and L_τ are the muon and tau lepton numbers, respectively. Therefore, the complete gauged group is $SU(3)_C \times SU(2)_L \times U(1)_Y \times U(1)_{L_\mu-L_\tau}$. The SM particle content has been extended by including three extra right-handed (RH) neutrinos and two SM gauge singlet scalars. All particles included in the $U(1)_{L_\mu-L_\tau}$ model and their charge assignments under various symmetry groups are listed in Table 1.

Table 1: Particle contents and corresponding charge assignments under various symmetry groups in the $U(1)_{L_\mu-L_\tau}$ model.

Gauge Group	Scalar Fields			Lepton Fields								
	φ_h	φ_H	φ_{DM}	L_e	L_μ	L_τ	e_R	μ_R	τ_R	N_R^e	N_R^μ	N_R^τ
$SU(2)_L$	2	1	1	2	2	2	1	1	1	1	1	1
$U(1)_Y$	1/2	0	0	-1/2	-1/2	-1/2	-1	-1	-1	0	0	0
$U(1)_{L_\mu-L_\tau}$	0	1	$n_{\mu\tau}$	0	1	-1	0	1	-1	0	1	-1

Gauge Group	Baryon Fields											
	u_L	d_L	c_L	s_L	t_L	b_L	u_R	d_R	c_R	s_R	t_R	b_R
$SU(2)_L$	2	2	2	2	2	2	1	1	1	1	1	1
$U(1)_Y$	1/6	1/6	1/6	1/6	1/6	1/6	2/3	-1/3	2/3	-1/3	2/3	-1/3
$U(1)_{L_\mu-L_\tau}$	0	0	0	0	0	0	0	0	0	0	0	0

The Lagrangian of the $U(1)_{L_\mu-L_\tau}$ model is as follows

$$\mathcal{L} = \mathcal{L}_{SM} + \mathcal{L}_N + \mathcal{L}_{DM} + |D_\nu \varphi_H|^2 - V - \frac{1}{4} F_{\mu\tau}^{\rho\sigma} F_{\mu\tau\rho\sigma} . \quad (1)$$

In above equation we have ignored the kinetic-mixing term between the groups $U(1)_Y$ and $U(1)_{L_\mu-L_\tau}$ in the case of assuming that the mixing is very small. The terms \mathcal{L}_{SM} , \mathcal{L}_N and \mathcal{L}_{DM} represent the SM, right hand (RH) neutrino and DM sectors, respectively. Since the processes we are studying do not involve RH neutrinos, its specific form is not given here. \mathcal{L}_{DM} represents the dark sector Lagrangian including the kinetic term of the DM candidate φ_{DM} and the interaction terms of φ_{DM} with the scalars fields φ_h and φ_H . The expression of \mathcal{L}_{DM} is given by

$$\begin{aligned} \mathcal{L}_{DM} = & (D^\nu \varphi_{DM})^\dagger (D_\nu \varphi_{DM}) - \mu_{DM}^2 \varphi_{DM}^\dagger \varphi_{DM} - \lambda_{DM} (\varphi_{DM}^\dagger \varphi_{DM})^2 \\ & - \lambda_{Dh} (\varphi_{DM}^\dagger \varphi_{DM}) (\varphi_h^\dagger \varphi_h) - \lambda_{DH} (\varphi_{DM}^\dagger \varphi_{DM}) (\varphi_H^\dagger \varphi_H) , \end{aligned} \quad (2)$$

where the parameters λ_{DM} , λ_{Dh} and λ_{DH} are quartic couplings of the scalar fields. As these couplings are feeble ($\sim 10^{-12}$) [37], the DM can not attain thermal equilibrium with the

thermal soup, which is called the Feebly Interacting Massive Particle (FIMP). In Eq. (1), the covariant derivatives involving in the kinetic energy term $|D_\nu \varphi_H|^2$ of the extra Higgs singlet φ_H can be expressed in a generic form $D_\nu \phi = (\partial_\nu + ig_{\mu\tau} Q_{\mu\tau}(\phi) Z_{\mu\tau\nu})\phi$, where ϕ is any SM single field which has $U(1)_{L_\mu-L_\tau}$ charge $Q_{\mu\tau}(\phi)$ (listed in Table 1) and $g_{\mu\tau}$ represents $U(1)_{L_\mu-L_\tau}$ group's gauge coupling constant. The scalar potential V contains all the self interactions of φ_H and its interactions with SM Higgs doublet. Its expression form is given by

$$V = \mu_H^2 \varphi_H^\dagger \varphi_H + \lambda_H (\varphi_H^\dagger \varphi_H)^2 + \lambda_{hH} (\varphi_h^\dagger \varphi_h) (\varphi_H^\dagger \varphi_H). \quad (3)$$

The last term in Eq. (1) represents the kinetic term for the additional gauge boson $Z_{\mu\tau}$ in terms with field strength tensor $F_{\mu\tau}^{\rho\sigma} = \partial^\rho Z_{\mu\tau}^\sigma - \partial^\sigma Z_{\mu\tau}^\rho$ of the $U(1)_{L_\mu-L_\tau}$ gauge group. When the scalar field φ_H has a non-zero of VEV, the $U(1)_{L_\mu-L_\tau}$ symmetry breaks spontaneously and consequently the corresponding new gauge boson $Z_{\mu\tau}$ obtains the mass $M_{Z_{\mu\tau}} = g_{\mu\tau} v_{\mu\tau}$. The SM Higgs doublet φ_h and the new scalar φ_H take the following form

$$\varphi_h = \begin{pmatrix} \tilde{H} \\ \frac{v+H+ia}{\sqrt{2}} \end{pmatrix}, \quad \varphi_H = \begin{pmatrix} \frac{v_{\mu\tau}+H_{\mu\tau}+ia}{\sqrt{2}} \end{pmatrix}, \quad (4)$$

where \tilde{H} , A and a are the massless Nambu-Goldstone Bosons (NGBs) absorbed by the gauge bosons W^\pm , Z and $Z_{\mu\tau}$, while v and $v_{\mu\tau}$ are the VEVs of the scalars φ_h and φ_H , respectively. Furthermore, H and $H_{\mu\tau}$ represent the physical CP-even scalar bosons. When both φ_h and φ_H obtain their respective VEVs, there will be a mass mixing between the states H and $H_{\mu\tau}$. The square of scalar mass matrix with off-diagonal elements proportional to λ_{hH} is given by

$$\mathcal{M}_{scalar}^2 = \begin{pmatrix} 2\lambda_h v^2 & \lambda_{hH} v_{\mu\tau} v \\ \lambda_{hH} v_{\mu\tau} v & 2\lambda_H v_{\mu\tau}^2 \end{pmatrix}. \quad (5)$$

Rotating the basis states H and $H_{\mu\tau}$ by a suitable angle α , we can make the above mass matrix diagonal. The new basis states (h_1 and h_2), now representing two physical states, are the linear combinations of H and $H_{\mu\tau}$ with the mixing angle α between H and $H_{\mu\tau}$, which can be expressed as

$$h_1 = H \cos \alpha + H_{\mu\tau} \sin \alpha, \quad h_2 = -H \sin \alpha + H_{\mu\tau} \cos \alpha, \quad (6)$$

$$\tan 2\alpha = \frac{\lambda_{hH} v_{\mu\tau} v}{\lambda_h v^2 - \lambda_H v_{\mu\tau}^2}. \quad (7)$$

When $\alpha \ll 1$, h_1 can be identified as the SM-like Higgs boson which has already been discovered by the CMS [1] and ATLAS [2] collaborations in 2012. h_2 is a new scalar particle. The masses of these two physical scalars h_1 and h_2 are given by

$$\begin{aligned} M_{h_1}^2 &= \sqrt{v^2 v_{\mu\tau}^2 (\lambda_{hH}^2 - 2\lambda_h \lambda_H) + \lambda_h^2 v^4 + \lambda_H^2 v_{\mu\tau}^4 + \lambda_h v^2 + \lambda_H v_{\mu\tau}^2}, \\ M_{h_2}^2 &= -\sqrt{v^2 v_{\mu\tau}^2 (\lambda_{hH}^2 - 2\lambda_h \lambda_H) + \lambda_h^2 v^4 + \lambda_H^2 v_{\mu\tau}^4 + \lambda_h v^2 + \lambda_H v_{\mu\tau}^2}. \end{aligned} \quad (8)$$

In this paper, we will assume that the values of M_{h_1} and v are fixed at 125 GeV and 246 GeV, respectively.

On one hand, compared with the SM Higgs boson, the couplings of h_1 with the SM particles are suppressed by a factor $\cos \alpha$ in the $U(1)_{L_\mu-L_\tau}$ model. Some relevant couplings of the SM-like Higgs boson h_1 with the SM particles, the new gauge boson $Z_{\mu\tau}$ and the DM candidate φ_{DM} are given by

$$\begin{aligned} g_{Z_{\mu\tau}Z_{\mu\tau}h_1} &= \frac{2M_{Z_{\mu\tau}}^2}{v_{\mu\tau}} \sin \alpha, \quad g_{f\bar{f}h_1} = -\frac{M_f}{v} \cos \alpha, \quad g_{VVh_1} = \frac{2M_V^2}{v} \cos \alpha, \\ g_{\varphi_{DM}^\dagger \varphi_{DM} h_1} &= -(v\lambda_{Dh} \cos \alpha + v_{\mu\tau}\lambda_{DH} \sin \alpha), \end{aligned} \quad (9)$$

where f represents all of the SM fermions and V represents the electroweak gauge bosons W^\pm or Z . On the other hand, similar with h_1 , the scalar h_2 can couple to all the SM particles and other new particles, such as new gauge boson $Z_{\mu\tau}$ and the DM particle φ_{DM} . Here, we also list the h_2 couplings, which are related our calculation

$$\begin{aligned} g_{Z_{\mu\tau}Z_{\mu\tau}h_2} &= \frac{2M_{Z_{\mu\tau}}^2}{v_{\mu\tau}} \cos \alpha, \quad g_{f\bar{f}h_2} = \frac{M_f}{v} \sin \alpha, \quad g_{VVh_2} = -\frac{2M_V^2}{v} \sin \alpha, \\ g_{\varphi_{DM}^\dagger \varphi_{DM} h_2} &= (v\lambda_{Dh} \sin \alpha - v_{\mu\tau}\lambda_{DH} \cos \alpha), \\ g_{h_1h_1h_2} &= 6v\lambda_h \cos^2 \alpha \sin \alpha - 6v_{\mu\tau}\lambda_H \sin^2 \alpha \cos \alpha - 2v\lambda_{hH} \sin \alpha \\ &\quad + 6v\lambda_{hH} \sin^3 \alpha - v_{\mu\tau}\lambda_{hH} \cos \alpha + 3v_{\mu\tau}\lambda_{hH} \sin^2 \alpha \cos \alpha. \end{aligned} \quad (10)$$

In the $U(1)_{L_\mu-L_\tau}$ model, $Z_{\mu\tau}$ has a light mass and no couplings to the SM quarks and the first generation leptons, so it can only decay to neutrinos. The couplings of $Z_{\mu\tau}$ with neutrinos are expressed as

$$g_{Z_{\mu\tau} \nu_\mu \nu_\mu} = \frac{M_{Z_{\mu\tau}}}{v_{\mu\tau}}, \quad g_{Z_{\mu\tau} \nu_\tau \nu_\tau} = -\frac{M_{Z_{\mu\tau}}}{v_{\mu\tau}}. \quad (11)$$

Taking no account of the neutrino masses, the expression form of the total decay width of $Z_{\mu\tau}$ is given by

$$\Gamma_{Z_{\mu\tau}} = \frac{g_{\mu\tau}^2 M_{Z_{\mu\tau}}}{12\pi}, \quad (12)$$

where we have also ignored the neutrino mixing.

To produce the appropriate neutrino mass and explain the muon $(g-2)$ anomaly, Ref. [36] has show the favored regions of the gauge coupling $g_{\mu\tau}$ and the $Z_{\mu\tau}$ mass, which are summarized as

$$g_{\mu\tau} \simeq [2 \times 10^{-4}, 2 \times 10^{-3}], \quad M_{Z_{\mu\tau}} \simeq [5, 210] \text{ MeV}. \quad (13)$$

According to Eq. (13), the range of $v_{\mu\tau}$ is given by

$$v_{\mu\tau} = \frac{M_{Z_{\mu\tau}}}{g_{\mu\tau}} \simeq [10, 1000] \text{ GeV}, \quad (14)$$

which indicates that, after the spontaneous symmetry breaking, the new scalar h_2 obtains mass as the same order with $v_{\mu\tau}$.

From above discussions we can see that, besides decaying to SM particles, the SM-like Higgs boson h_1 has extra decay modes $Z_{\mu\tau}Z_{\mu\tau}$ and $\varphi_{DM}^\dagger\varphi_{DM}$ for $M_{DM} < M_{h_1}$. The expressions of these decay channels are

$$\Gamma(h_1 \rightarrow Z_{\mu\tau}Z_{\mu\tau}) = \frac{g_{Z_{\mu\tau}Z_{\mu\tau}h_1}^2 (M_{h_1}^4 - 4M_{Z_{\mu\tau}}^2 M_{h_1}^2 + 12M_{Z_{\mu\tau}}^4) \sqrt{M_{h_1}^2 - 4M_{Z_{\mu\tau}}^2}}{128\pi M_{h_1}^2 M_{Z_{\mu\tau}}^4}, \quad (15)$$

$$\Gamma(h_1 \rightarrow \varphi_{DM}^\dagger\varphi_{DM}) = \frac{g_{\varphi_{DM}^\dagger\varphi_{DM}h_1}^2}{32\pi M_{h_1}} \sqrt{1 - \frac{4M_{DM}^2}{M_{h_1}^2}}, \quad (16)$$

where the M_{DM} is Dark Matter mass. The total decay width of h_1 can be written as

$$\Gamma(h_1) = \cos^2 \alpha \Gamma_{SM} + \Gamma(h_1 \rightarrow Z_{\mu\tau}Z_{\mu\tau}) + \Gamma(h_1 \rightarrow \varphi_{DM}^\dagger\varphi_{DM}), \quad (17)$$

where Γ_{SM} is the total width of the Higgs boson in the SM. In the $U(1)_{L_\mu-L_\tau}$ model, the decays of φ_{DM} and $Z_{\mu\tau}$ are invisible, the branching ratio of the invisible decays is given by

$$BR(h_1 \rightarrow \text{invisibles}) = \frac{\Gamma(h_1 \rightarrow Z_{\mu\tau}Z_{\mu\tau}) + \Gamma(h_1 \rightarrow \varphi_{DM}^\dagger\varphi_{DM})}{\Gamma(h_1)}. \quad (18)$$

As we can see from Eq. (9) and Eq. (10), the couplings of φ_{DM} with scalar bosons h_1 and h_2 depend on the parameters λ_{Dh} and λ_{DH} . In this work, we take $\lambda_{Dh} = 9.8 \times 10^{-13}$ and $\lambda_{DH} = 1.3 \times 10^{-11}$ [37], which makes the $\Gamma(h_1 \rightarrow \varphi_{DM}^\dagger\varphi_{DM})$ and $\Gamma(h_2 \rightarrow \varphi_{DM}^\dagger\varphi_{DM})$ so feeble that they can be ignored. Using the constraint on the branching ratio of the Higgs invisible decay, $BR_{\text{invis}} \leq 0.24$ at 95% C. L. from the LHC data [55], the sine of scalar mixing angle $\sin \alpha$ must be satisfied $\sin \alpha \leq 0.3$. Then, for the factor χ , there is

$$\chi = \frac{\alpha}{v_{\mu\tau}} \leq 2.2 \times 10^{-4} \text{ GeV}^{-1}. \quad (19)$$

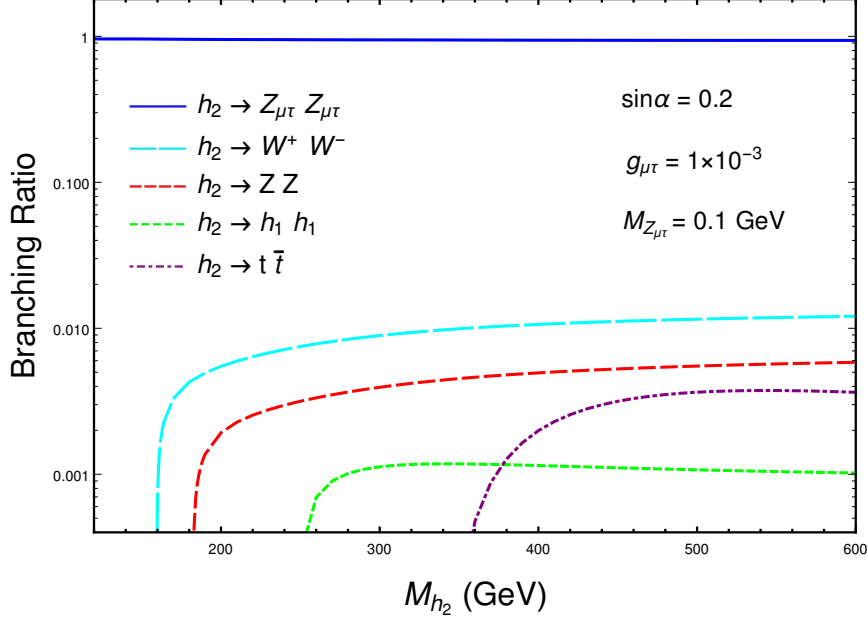
To summarize, in the $U(1)_{L_\mu-L_\tau}$ model, three new free parameters are introduced, which are the new gauge coupling constant $g_{\mu\tau}$, the $Z_{\mu\tau}$ mass $M_{Z_{\mu\tau}}$ and the scalar mixing angle α , respectively. In the following, we will focus our attention on the phenomenology of the new particles h_2 and $Z_{\mu\tau}$ at e-p colliders in the above allowed parameter space.

III. Decays and Productions of the Scalar h_2

3.1. Decays of the scalar h_2

In the $U(1)_{L_\mu-L_\tau}$ model, the scalar h_2 can not only decay to the SM particles but also decay to the new particles $Z_{\mu\tau}$ and φ_{DM} . Here, we give the decay width expressions of its several major decay modes. The expression form of the decay width for the decay channel $h_2 \rightarrow Z_{\mu\tau}Z_{\mu\tau}$ is given by

$$\Gamma(h_2 \rightarrow Z_{\mu\tau}Z_{\mu\tau}) = \frac{g_{Z_{\mu\tau}Z_{\mu\tau}h_2}^2 (M_{h_2}^4 - 4M_{Z_{\mu\tau}}^2 M_{h_2}^2 + 12M_{Z_{\mu\tau}}^4) \sqrt{M_{h_2}^2 - 4M_{Z_{\mu\tau}}^2}}{128\pi M_{h_2}^2 M_{Z_{\mu\tau}}^4}. \quad (20)$$



0

Figure 1: The branching ratios for the main decay modes of the scalar h_2 as functions of M_{h_2} for the fixed values $\sin\alpha = 0.2$, $M_{Z_{\mu\tau}} = 0.1$ GeV and $g_{\mu\tau} = 1 \times 10^{-3}$.

Under the assumption $\frac{M_{Z_{\mu\tau}}}{M_{h_1}} \rightarrow 0$, we can obtain the following form

$$\Gamma(h_2 \rightarrow Z_{\mu\tau} Z_{\mu\tau}) = \frac{M_{h_2}^3 \cos^2 \alpha}{32\pi v_{\mu\tau}^2}. \quad (21)$$

The decay width of the channel $h_2 \rightarrow \varphi_{DM}^\dagger \varphi_{DM}$ is

$$\Gamma(h_2 \rightarrow \varphi_{DM}^\dagger \varphi_{DM}) = \frac{g_{\varphi_{DM}^\dagger \varphi_{DM} h_2}^2}{16\pi M_{h_2}} \sqrt{1 - \frac{4M_{DM}^2}{M_{h_2}^2}}. \quad (22)$$

As we already mentioned, the value of $\Gamma(h_2 \rightarrow \varphi_{DM}^\dagger \varphi_{DM})$ is small enough and we will neglect it.

The width of h_2 decaying to vector bosons is given as

$$\Gamma(h_2 \rightarrow VV) = \frac{g_{Vh_2}^2 (M_{h_2}^4 - 4M_V^2 M_{h_2}^2 + 12M_V^4) \sqrt{M_{h_2}^2 - 4M_V^2}}{64\pi S_V M_{h_2}^2 M_V^4}, \quad (23)$$

where S_V represents the statistical factor. Its value equals to 1 for W^\pm boson and 2 for Z boson.

The width for the decay process $h_2 \rightarrow h_1 h_1$ can be written as

$$\Gamma(h_2 \rightarrow h_1 h_1) = \frac{g_{h_1 h_1 h_2}^2 \sqrt{M_{h_2}^2 - 4M_{h_1}^2}}{32\pi M_{h_2}^2}. \quad (24)$$

From Eq. (10) one can see that the coupling constant $g_{h_1 h_1 h_2}$ depends on the couplings λ_h , λ_H and λ_{hH} , which are expressed as

$$\begin{aligned} \lambda_H &= \frac{M_{h_2}^2 + M_{h_1}^2 - (M_{h_1}^2 - M_{h_2}^2) \cos 2\alpha}{4v_{\mu\tau}^2}, \\ \lambda_h &= \frac{M_{h_2}^2 + M_{h_1}^2 - (M_{h_2}^2 - M_{h_1}^2) \cos 2\alpha}{4v^2}, \\ \lambda_{hH} &= -\frac{(M_{h_2}^2 - M_{h_1}^2) \cos \alpha \sin \alpha}{vv_{\mu\tau}}. \end{aligned} \quad (25)$$

When we take $\sin \alpha = 0.2$ and $v_{\mu\tau} = \frac{M_{Z_{\mu\tau}}}{g_{\mu\tau}} = 100$ GeV, the decay width $\Gamma(h_2 \rightarrow h_1 h_1)$ only depends on M_{h_2} .

The width of h_2 decaying to the SM fermion pair is given as

$$\Gamma(h_2 \rightarrow f\bar{f}) = \frac{n_c g_{ffh_2} (M_{h_2}^2 - 4M_f^2)^{\frac{3}{2}}}{8\pi M_{h_2}^2}, \quad (26)$$

where the color charge $n_c = 1$ for leptons and 3 for quarks. Fig. 1 shows the branching ratios for the main decay modes of the scalar h_2 as functions of the mass parameter M_{h_2} for the fixed values $\sin \alpha = 0.2$, $M_{Z_{\mu\tau}} = 0.1$ GeV and $g_{\mu\tau} = 1 \times 10^{-3}$, where the curves from high to low correspond the $Z_{\mu\tau} Z_{\mu\tau}$ decay modes, the $W^+ W^- / ZZ$ decay modes, di-higgs decay mode and di-top decay mode, respectively. One can see from this figure that the value of the branching ratio $BR(h_2 \rightarrow Z_{\mu\tau} Z_{\mu\tau})$ is about 98% and only is 2% for the rest decay channels. Certainly, the values of these branching ratios would vary as the values of the parameters $\sin \alpha$ and $g_{\mu\tau}$ changing. However, in the allowed parameter space of the $U(1)_{L_\mu - L_\tau}$ model, the decay process $h_2 \rightarrow Z_{\mu\tau} Z_{\mu\tau}$ is the main decay channel of the scalar h_2 .

3.2. Productions of the scalar h_2

Like the SM Higgs boson, the additional scalar h_2 in the $U(1)_{L_\mu - L_\tau}$ model is produced via two major channels: the charged current (CC) production channel via $W^+ W^-$ fusion and the neutral current (NC) production channel via ZZ fusion [56, 57] at e-p colliders. Fig. 2 gives the corresponding Feynman diagrams for the h_2 production via CC production channel and NC production channel at e-p colliders, respectively. Then, employing Madgraph5/aMC@NLO [58], we calculate the production cross sections of the processes $e^- p \rightarrow \nu_e j h_2$ and $e^- p \rightarrow e^- j h_2$ as functions of $M_{Z_{\mu\tau}}$ at the LHeC. It is well known that polarization of the initial state electron can affect the production cross sections. Our numerical results show that the beam polarization $P(e^-) = -0.8$ can maximize the cross sections. Therefore, we will take $P(e^-) = -0.8$ in following numerical calculation. Since $g_{\mu\tau}$ does not affect the cross sections of h_2 production via the CC and NC processes, we do not consider it here. In Figs. 3 (a) and 3 (b), the curves show the cross sections of the

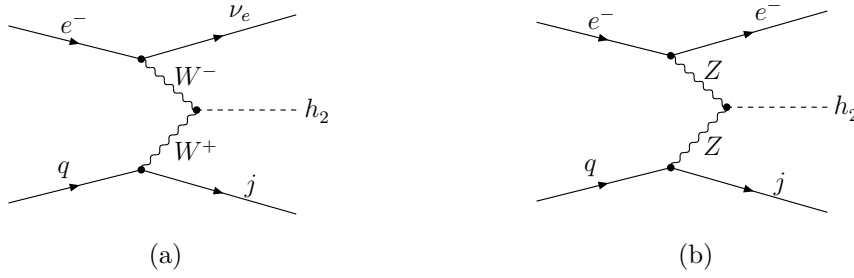


Figure 2: The Feynman diagrams for the scalar h_2 productions at e-p colliders (Left (a): CC production channel, Right (b): NC production channel).

$e^-p \rightarrow e^-jh_2$ and $e^-p \rightarrow \nu_ejh_2$ processes with $E_{e^-} = 140$ GeV and different values of mixing angle $\sin \alpha = 0.2$ (solid), 0.05 (dashed) and 0.01 (dotted). One can see from these figures that the values of the production cross section σ decrease as the h_2 mass increases. For the $e^-p \rightarrow e^-jh_2$ process and $10 \text{ GeV} \leq M_{h_2} \leq 1000 \text{ GeV}$, its values are in the ranges of $1.73 \text{ pb} \times 10^{-6} \leq \sigma \leq 4.33 \times 10^{-3} \text{ pb}$ (solid), $1.08 \times 10^{-7} \text{ pb} \leq \sigma \leq 2.71 \times 10^{-4} \text{ pb}$ (dashed) and $4.33 \times 10^{-9} \text{ pb} \leq \sigma \leq 1.08 \times 10^{-5} \text{ pb}$ (dotted), respectively. For the $e^-p \rightarrow \nu_ejh_2$ process and $10 \text{ GeV} \leq M_{h_2} \leq 1000 \text{ GeV}$, its values are in the ranges of $1.77 \times 10^{-5} \text{ pb} \leq \sigma \leq 3.73 \times 10^{-2} \text{ pb}$ (solid), $1.11 \times 10^{-6} \text{ pb} \leq \sigma \leq 2.33 \times 10^{-3} \text{ pb}$ (dashed) and $4.43 \times 10^{-8} \text{ pb} \leq \sigma \leq 9.32 \times 10^{-5} \text{ pb}$ (dotted) respectively. It is worth mentioning that the cross section of the $e^-p \rightarrow \nu_ejh_2$ process is larger than that of the $e^-p \rightarrow e^-jh_2$ process by about one order of magnitude.

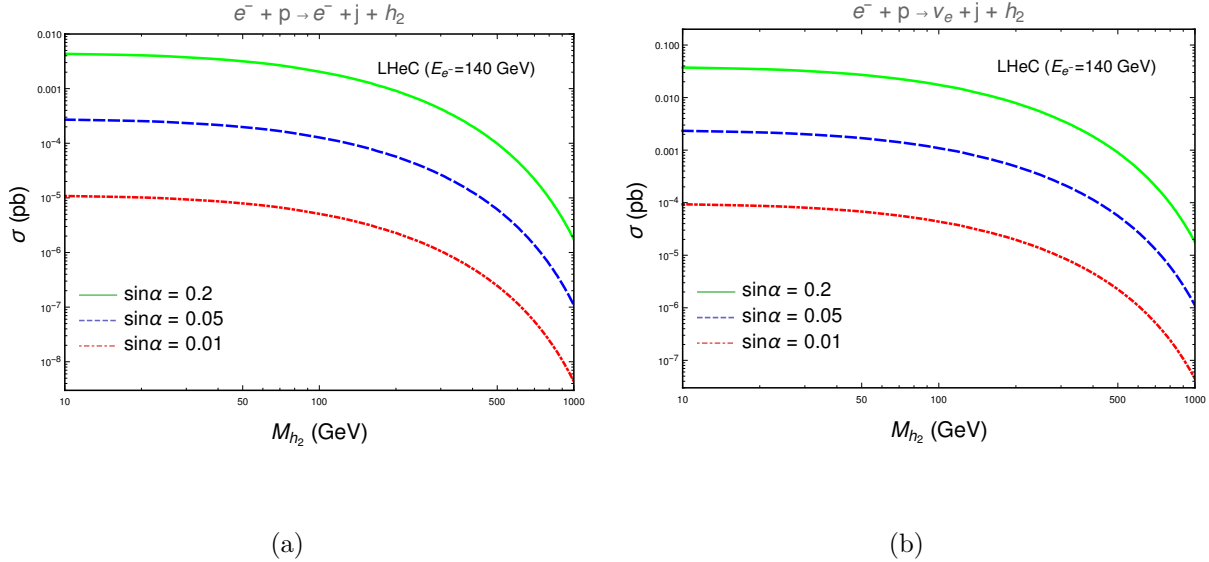


Figure 3: The production cross sections of the processes $e^-p \rightarrow e^-jh_2$ and $e^-p \rightarrow \nu_ejh_2$ as functions of the mass parameter M_{h_2} for $\sin \alpha = 0.2$ (solid), 0.05 (dashed), 0.01 (dotted) and the beam polarization $P(e^-) = -0.8$ at the LHeC.

IV. Productions of the New Gauge Boson $Z_{\mu\tau}$

Now, we turn our attention to the new gauge boson $Z_{\mu\tau}$. As mentioned in the previous section, $Z_{\mu\tau}$ can not establish couplings with all the SM quarks and the first generation leptons, making it very difficult to be produced directly. So it is a attractive scheme to obtain $Z_{\mu\tau}$ by considering its indirect production. Similar with the new scalar h_2 , besides decaying to the SM particles, the SM-like Higgs boson h_1 can also decay to a pair of $Z_{\mu\tau}$. Eq. (15) has given the expression form of the decay width $\Gamma(h_1 \rightarrow Z_{\mu\tau}Z_{\mu\tau})$, which can be simplified to

$$\Gamma(h_1 \rightarrow Z_{\mu\tau}Z_{\mu\tau}) = \frac{M_{h_1}^3 \sin^2 \alpha}{32\pi v_{\mu\tau}^2}. \quad (27)$$

From above equation we can see that the production rate of the $Z_{\mu\tau}$ pair from h_1 decaying is actually determined by the factor $\chi^2 \simeq \sin^2 \alpha / v_{\mu\tau}^2$. So, in this work, all the results for the $Z_{\mu\tau}$ production via h_1 decaying can be expressed as functions of the factor χ . Next, we will consider its indirect productions via the decays of h_2 and h_1 , respectively.

As can be seen from Fig. 3, the CC production of scalar h_2 has larger cross section than that for its NC production. However, as mentioned earlier, $Z_{\mu\tau}$ can only decay to neutrinos in the $U(1)_{L_\mu-L_\tau}$ model. So the final states of the $e^-p \rightarrow \nu_e j h_2 (h_2 \rightarrow Z_{\mu\tau}Z_{\mu\tau})$ and $e^-p \rightarrow \nu_e j h_1 (h_1 \rightarrow Z_{\mu\tau}Z_{\mu\tau})$ processes would be jets and missing energy, which are difficult to be distinguished from the deeply inelastic scattering (DIS) backgrounds. Moreover, lack of kinematic handles in the final state makes it extremely difficult to filter signal from many backgrounds. Therefore, in this work we will focus on the NC production channels $e^-p \rightarrow e^- j h_1 (\rightarrow Z_{\mu\tau}Z_{\mu\tau}) \rightarrow e^- j + \cancel{E}_T$ and $e^-p \rightarrow e^- j h_2 (\rightarrow Z_{\mu\tau}Z_{\mu\tau}) \rightarrow e^- j + \cancel{E}_T$ to study the feasibility of detecting h_2 and $Z_{\mu\tau}$. In Fig. 4, we show the leading order Feynman diagrams of the $Z_{\mu\tau}$ productions by the decays of h_1 and h_2 at e-p colliders.

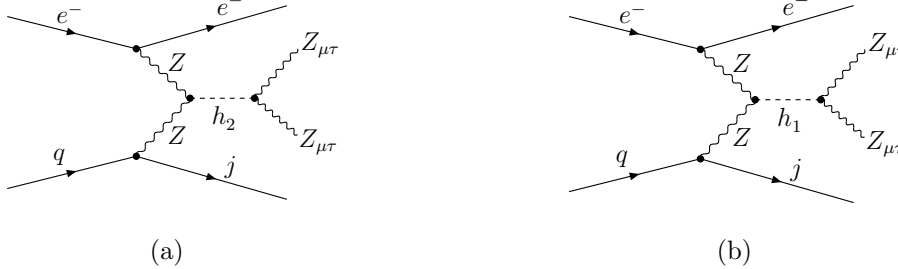


Figure 4: The leading order Feynman diagrams of the $Z_{\mu\tau}$ productions by the decays of h_1 and h_2 via the NC production channels at e-p colliders.

Employing the Madgraph5/aMC@NLO [58], we calculate the cross sections of the $Z_{\mu\tau}$ production processes $e^-p \rightarrow e^- j h_2 \rightarrow e^- j Z_{\mu\tau}Z_{\mu\tau}$ and $e^-p \rightarrow e^- j h_1 \rightarrow e^- j Z_{\mu\tau}Z_{\mu\tau}$. Considering the favored region of the parameter space to resolve $(g-2)_\mu$ discrepancy, $g_{\mu\tau}$ is fixed to $g_{\mu\tau} = 1 \times 10^{-3}$ for reference. Due to $BR(h_2 \rightarrow Z_{\mu\tau}Z_{\mu\tau}) \sim 1$, the cross section of the $Z_{\mu\tau}$ production via h_2 decaying as a function of the mass M_{h_2} for $\sin \alpha = 0.2, 0.05$ and 0.01 at LHeC with $E_{e^-} = 140$ GeV is essentially the same as Fig. 3 (a). So we don't show it again. Fig. 5 shows the cross sections of the $Z_{\mu\tau}$ production by h_1 decaying as functions of the factor χ at e-p colliders, where the different curves show the $Z_{\mu\tau}$ production

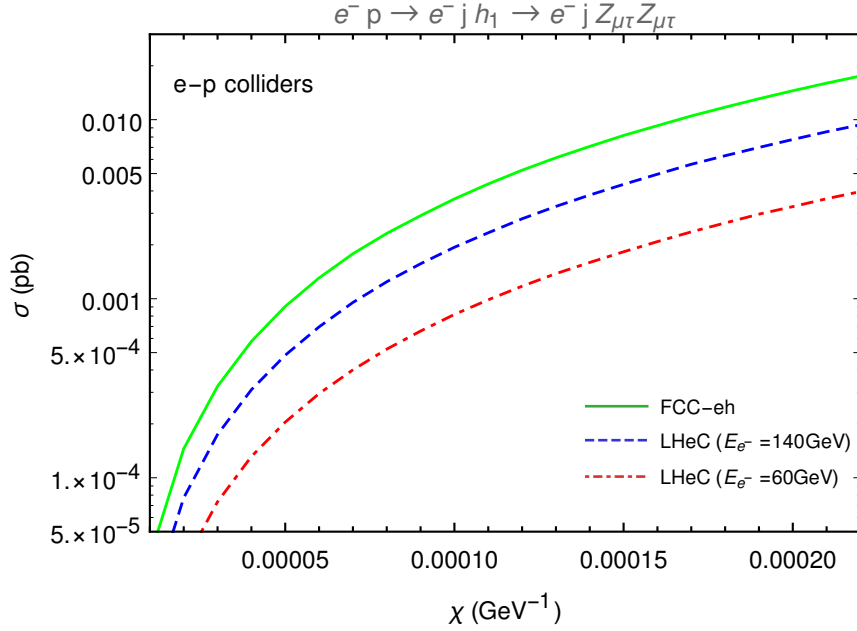


Figure 5: The production cross sections of the process $e^-p \rightarrow e^-j h_1 \rightarrow e^-j Z_{\mu\tau} Z_{\mu\tau}$ as functions of χ at e-p colliders.

cross sections at different colliders: FCC-eh (solid), LHeC with $E_{e^-} = 140$ GeV (dashed) and LHeC with $E_{e^-} = 60$ GeV (dotted). From Fig. 5, we can see that, for $1 \times 10^{-5} \text{ GeV} \leq \chi \leq 2 \times 10^{-4} \text{ GeV}$, the values of the $Z_{\mu\tau}$ production cross sections are in the ranges $3.61 \times 10^{-5} \text{ pb} \leq \sigma \leq 1.75 \times 10^{-2} \text{ pb}$ (solid), $1.94 \times 10^{-5} \text{ pb} \leq \sigma \leq 9.37 \times 10^{-3} \text{ pb}$ (dashed) and $8.16 \times 10^{-6} \text{ pb} \leq \sigma \leq 3.97 \times 10^{-3} \text{ pb}$ (dotted).

V. Signatures of the New Particles h_2 and $Z_{\mu\tau}$ at e-p Colliders

In this section, we analyze the observation potential by performing a Monte Carlo simulation of the signal and background events and explore the observability of the additional scalar h_2 and the new gauge boson $Z_{\mu\tau}$ at e-p colliders with the integrated luminosity of 1 ab^{-1} . On one hand, we will explore the observability of h_2 as well as $Z_{\mu\tau}$ via the processes $e^-p \rightarrow e^-j h_2 \rightarrow e^-j Z_{\mu\tau} Z_{\mu\tau}$ and $e^-p \rightarrow e^-j h_1 \rightarrow e^-j Z_{\mu\tau} Z_{\mu\tau}$. For the second process, we mainly use it to explore the signature of $Z_{\mu\tau}$. On the other hand, for more comprehensive, we will also analysis the possibility of detecting h_2 through CC production channel followed by h_2 decaying into vector boson pair (ZZ).

We use Madgraph5/aMC@NLO [58] to calculate the relevant production cross sections and generate the signal and background events, where the UFO format of the $U(1)_{L_\mu-L_\tau}$ model has been obtained by using FeynRules [59]. Moreover, the parton distribution function (PDF), NNPDF2.3 [60], is used at leading order and Pythia-pgs [61] is employed for parton showering, hadronization and fast detector simulation. Finally, MadAnalysis5 [62] is applied for data analysis and plotting. All of the SM input parameters are taken from Particle Data Group (PDG) [63].

A. $h_2 \rightarrow Z_{\mu\tau}Z_{\mu\tau}$ and $h_1 \rightarrow Z_{\mu\tau}Z_{\mu\tau}$ Channels

In this subsection, we take both h_2 and h_1 productions at e-p colliders through NC production channels followed by $h_2 \rightarrow Z_{\mu\tau}Z_{\mu\tau}$ and $h_1 \rightarrow Z_{\mu\tau}Z_{\mu\tau}$ as our signals, signal-1 and signal-2, respectively. Since $Z_{\mu\tau}$ has invisible final state in the detector, these two processes provide the same final state that includes one electron, one jet and a large missing transverse energy \cancel{E}_T

$$e^- + p \rightarrow e^- + j + h_2(\rightarrow Z_{\mu\tau}Z_{\mu\tau}) \rightarrow e^- + j + \cancel{E}_T, \text{ (signal - 1)} \quad (28)$$

$$e^- + p \rightarrow e^- + j + h_1(\rightarrow Z_{\mu\tau}Z_{\mu\tau}) \rightarrow e^- + j + \cancel{E}_T, \text{ (signal - 2)} \quad (29)$$

in which \cancel{E}_T comes from $Z_{\mu\tau} \rightarrow \nu\bar{\nu}$. For $\sin\alpha = 0.2$ and $g_{\mu\tau} = 1 \times 10^{-3}$, the values of the cross section for the signal-1 are 4.179×10^{-4} pb (1.046×10^{-4} pb) for $E_{e^-} = 140$ (60) GeV at the LHeC and 9.251×10^{-4} pb at the FCC-eh. While the values of the cross section for the signal-2 are 1.898×10^{-3} pb (5.441×10^{-4} pb) for $E_{e^-} = 140$ (60) GeV at the LHeC and 2.412×10^{-3} pb at the FCC-eh for $\chi = 9 \times 10^{-5}$ GeV $^{-1}$.

For the signal $e^-j\cancel{E}_T$, the leading irreducible SM backgrounds can be classified into two general categories. The first category has a final state $e^-j\nu_e\bar{\nu}_e$ which comes from the following two processes

$$e^- + p \rightarrow W^-(\rightarrow e^-\bar{\nu}_e) + j + \nu_e \rightarrow e^- + j + \cancel{E}_T (e^-j\nu_e\bar{\nu}_e), \quad (30)$$

$$e^- + p \rightarrow Z(\rightarrow \nu_e\bar{\nu}_e) + j + e^- \rightarrow e^- + j + \cancel{E}_T (e^-j\nu_e\bar{\nu}_e). \quad (31)$$

The total cross section for this kind of irreducible backgrounds is 0.4334 pb (0.205 pb) for $E_{e^-} = 140$ (60) GeV at the LHeC and 0.8116 pb at the FCC-eh, which will severely pollute the physical signal.

The second category has a final state $e^-j\nu_{\mu,\tau}\bar{\nu}_{\mu,\tau}$

$$e^- + p \rightarrow Z(\rightarrow \nu_{\mu,\tau}\bar{\nu}_{\mu,\tau}) + j + e^- \rightarrow e^- + j + \cancel{E}_T (e^-j\nu_{\mu,\tau}\bar{\nu}_{\mu,\tau}). \quad (32)$$

Its production cross section is 0.05685 pb (0.03422 pb) for $E_{e^-} = 140$ (60) GeV at the LHeC and 0.1052 pb at the FCC-eh. Besides, more remarkably, the photoproduction of the state $W + j$, which has a larger cross section, is also an irreducible SM background if the W boson decays to an electron and neutrino. But it can be negligible after all selection cuts, because of its unique kinematic features.

There are also some reducible backgrounds which come from various sources. The most threatening reducible backgrounds result from the production of τ in the final state. One is

$$e^- + p \rightarrow e^- + j + \tau^+ + \nu_\tau (e^-j\tau^+\nu_\tau). \quad (33)$$

Its cross section is 0.264 pb (0.1331 pb) for $E_{e^-} = 140$ (60) GeV at the LHeC and 0.3957 pb at the FCC-eh. The other one is

$$e^- + p \rightarrow e^- + j + \tau^- + \bar{\nu}_\tau (e^-j\tau^-\bar{\nu}_\tau). \quad (34)$$

Its cross section is 0.2816 pb (0.1362 pb) for $E_{e^-} = 140$ (60) GeV at the LHeC and 0.5015 pb at the FCC-eh. The main reasons why the above two processes (Eq. (33) and Eq. (34))

can be viewed as reducible backgrounds are: (I) The τ -jets may be misidentified as hadronic jets. (II) The detection of hadronic decay products of τ cannot be expected to be fully efficient due to the products being too soft, which will lead to generation of the missing energy \cancel{E}_T . Furthermore, we can even consider the case (II) as a source of partial irreducible background. The $e^-p \rightarrow \nu_e j \tau^+ \nu_\tau$ and $e^-p \rightarrow \nu_e j \tau^- \bar{\nu}_\tau$ processes are reducible backgrounds in which the τ decays to an electron. Fortunately, we could suppress them to an insignificant order because of the totally different kinematic distribution of the final electron. Some other reducible backgrounds are e +multijet productions in which the \cancel{E}_T comes from jet's mismeasurement and $jj\nu$ production in which one jet is misidentified as an electron. In this work, we do not simulate both of them because their contributions can be negligible after all selection cuts. The signal and background events are generated with following basic cuts [56] in Madgraph5/aMC@NLO [58]

- lepton transverse momentum $p_T(l^\pm) > 5$ GeV,
- jet transverse momentum $p_T(j) > 20$ GeV,
- lepton pseudorapidity in the range $|\eta(l^\pm)| < 5$,
- jet pseudorapidity in the range $|\eta(j)| < 5$,
- angular separation between jet and lepton $\Delta R(jl^\pm) > 0.4$,

where $\eta = 1/2 \ln(\tan \theta)$ is the pseudorapidity, where θ indicates the scattering angle in the laboratory frame. $\Delta R = \sqrt{(\Delta\phi)^2 + (\Delta\eta)^2}$ is the particle separation, where $\Delta\phi$ and $\Delta\eta$ represent the rapidity gap and the azimuthal angle gap between the particle pair, respectively.

Table 2: Effect of individual kinematical cuts on the signal-1 for $M_{h_2} = 300$ GeV, $M_{Z_{\mu\tau}} = 0.1$ GeV, $\sin\alpha = 0.2$ and $g_{\mu\tau} = 1 \times 10^{-3}$ and the SM backgrounds at the LHeC with $E_{e^-} = 140$ (60) GeV. The statistical significance is computed for the integrated luminosity as 1 ab^{-1} .

LHeC,	$E_{e^-} = 140$ (60) GeV,	$E_p = 7$ TeV	
cuts	signal (S)	total background (B)	$S/\sqrt{S+B}$
initial (no cut)	417.0 (104.0)	1.01×10^6 (5.09×10^5)	0.41 (0.15)
basic cuts	392.1 (97.6)	8.53×10^5 (4.11×10^5)	0.42 (0.16)
$\cancel{E}_T < 20$ ($\cancel{E}_T < 20$) GeV	238.6 (70.7)	5.17×10^4 (4.89×10^4)	1.05 (0.32)
TET > 300 (TET > 260) GeV	235.9 (64.6)	1.65×10^4 (4.63×10^3)	1.83 (0.94)
THT > 200 (THT > 200) GeV	235.7 (63.8)	9.91×10^3 (1.42×10^3)	2.30 (1.65)
$E_T(jj) > 100$ ($E_T(jj) > 90$) GeV	232.7 (60.4)	7.83×10^3 (1.08×10^3)	2.59 (1.79)
$E_T(e^-j) > 150$ ($E_T(e^-j) > 120$) GeV	232.3 (59.5)	7.44×10^3 (9.93×10^2)	2.65 (1.84)

After the basic cuts, we further employ optimized kinematical cuts on separating the signals from the SM backgrounds. In our theoretical framework, although the SM backgrounds have a huge effect on the signals, there are many kinematical differences between them that can be exploited. In Fig. 6, we show the normalized distributions of the total missing transverse energy \cancel{E}_T , the visible transverse energy TET, the missing transverse hadronic energy

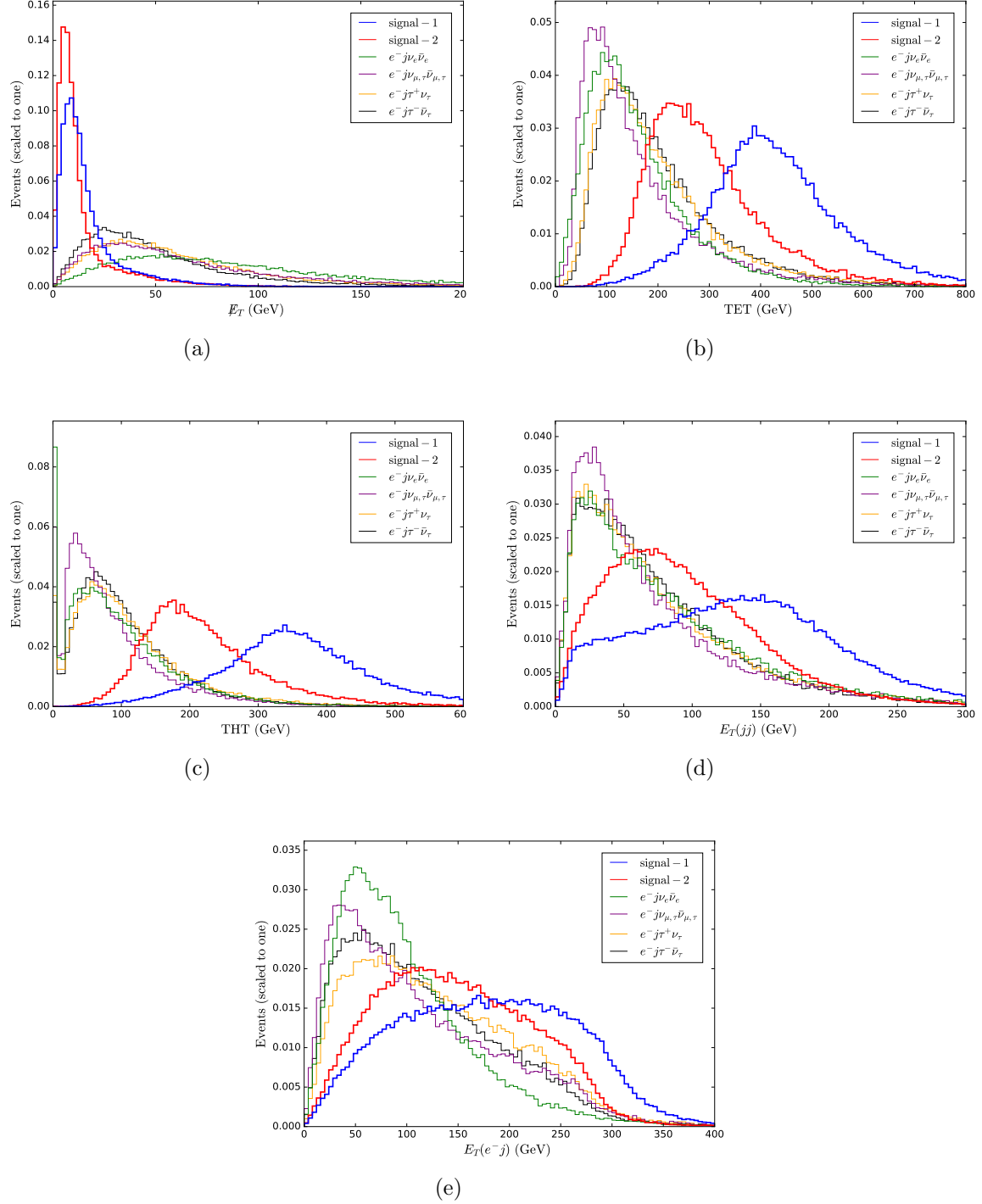


Figure 6: Normalized distributions of \cancel{E}_T (a), TET (b), THT (c), $E_T(jj)$ (d) and $E_T(e^-j)$ (e) for the signals and backgrounds at the LHeC with $E_{e^-} = 140$ GeV and an integrated luminosity of 1 ab^{-1} .

Table 3: Effect of individual kinematical cuts on the signal-2 for $M_{Z_{\mu\tau}} = 0.1$ GeV and $\chi = 9 \times 10^{-5}$ GeV $^{-1}$ and the SM backgrounds at the LHeC with $E_{e^-} = 140$ (60) GeV. The statistical significance is computed for the integrated luminosity as 1 ab $^{-1}$.

LHeC, $E_{e^-} = 140$ (60) GeV, $E_p = 7$ TeV			
cuts	signal (S)	total background (B)	$S/\sqrt{S+B}$
initial (no cut)	1288.0 (544.0)	1.01×10^6 (5.09×10^5)	1.28 (0.76)
basic cuts	1205.9 (508.1)	8.53×10^5 (4.11×10^5)	1.30 (0.79)
$\cancel{E}_T < 20$ ($\cancel{E}_T < 18$) GeV	980.9 (386.0)	8.79×10^4 (4.05×10^4)	3.29 (1.91)
TET > 200 (TET > 160) GeV	827.7 (361.9)	2.26×10^4 (1.27×10^4)	5.41 (3.16)
THT > 140 (THT > 120) GeV	808.1 (354.3)	1.20×10^4 (6.09×10^3)	7.14 (4.41)
$E_T(jj) > 60$ ($E_T(jj) > 60$) GeV	803.5 (374.8)	9.65×10^3 (4.46×10^3)	7.86 (5.02)
$E_T(e^-j) > 100$ ($E_T(e^-j) > 80$) GeV	796.1 (343.7)	8.96×10^3 (4.19×10^3)	8.06 (5.10)

THT, jet pair transverse energy $E_T(jj)$ and electron jet transverse energy $E_T(e^-j)$ for the signals and backgrounds at the LHeC with $E_{e^-} = 140$ GeV and an integrated luminosity of 1 ab $^{-1}$. From these figures, we can see that the distributions of signals have good distinctions from the distributions of the relevant backgrounds (peaks locate in different locations). In principle, there are other variables which we can use to discriminate the signals from backgrounds. But, these variables are remarkably similar and can not work significantly better than above kinematic variables. After all these kinematical cuts are applied, the event numbers of signal-1, signal-2 and corresponding backgrounds are summarized in Table 2 and Table 3 for the LHeC with $E_{e^-} = 140$ (60) GeV, respectively. The values of the statistical significance SS are also shown in these tables, which is defined as $SS = S/\sqrt{S+B}$ with S and B being the number of signal and background events, respectively.

Table 4: Effect of individual kinematical cuts on the signal-1 for $M_{h_2} = 300$ GeV, $M_{Z_{\mu\tau}} = 0.1$ GeV, $\sin\alpha = 0.2$ and $g_{\mu\tau} = 1 \times 10^{-3}$ and backgrounds at the FCC-eh. The statistical significance SS is computed for an integrated luminosity of 1 ab $^{-1}$.

FCC-eh, $E_{e^-} = 60$ GeV, $E_p = 50$ TeV			
cuts	signal (S)	total background (B)	$S/\sqrt{S+B}$
initial (no cut)	925.0	1.81×10^6	0.69
basic cuts	863.3	1.30×10^6	0.76
$\cancel{E}_T < 20$ GeV	303.2	1.29×10^5	0.84
TET > 280 GeV	279.1	1.35×10^4	2.38
THT > 200 GeV	277.7	7.34×10^3	3.18
$E_T(jj) > 100$ GeV	263.7	5.84×10^3	3.38
$E_T(e^-j) > 120$ GeV	261.9	5.61×10^3	3.42

On the other hand, it is well known that the FCC-eh collides electrons to protons with $E_{e^-} = 60$ GeV and $E_p = 50$ TeV, which is a typical deep inelastic facility with $\sqrt{s} \approx 3.5$ TeV. Therefore, we need to modify the above veto criteria and kinematic cuts to adjust the progressive detector simulation, because the FCC-eh has a higher proton beam energy than LHeC. The modified values for the kinematic cuts and the event numbers of signal-1, signal-2 and backgrounds are presented in Table 4 and Table 5, respectively.

From these tables, we can see that, for $\sin\alpha = 0.2$, $M_{Z_{\mu\tau}} = 0.1$ GeV, $M_{h_2} = 300$ GeV,

Table 5: Effect of individual kinematical cuts on the signal-2 for $M_{Z_{\mu\tau}} = 0.1$ GeV and $\chi = 9 \times 10^{-5}$ GeV $^{-1}$ and backgrounds at the FCC-eh. The statistical significance SS is computed for an integrated luminosity of 1 ab $^{-1}$.

FCC-eh, $E_{e^-} = 60$ GeV, $E_p = 50$ TeV			
cuts	signal (S)	total background (B)	$S/\sqrt{S+B}$
initial (no cut)	2412.0	1.82×10^6	1.79
basic cuts	2246.7	1.30×10^6	1.96
$\cancel{E}_T < 20$ GeV	1086.9	1.29×10^5	3.01
TET > 180 GeV	981.0	3.76×10^4	5.00
THT > 120 GeV	972.0	2.46×10^4	6.08
$E_T(jj) > 60$ GeV	959.3	1.92×10^4	6.76
$E_T(e^-j) > 80$ GeV	952.9	1.79×10^4	6.94

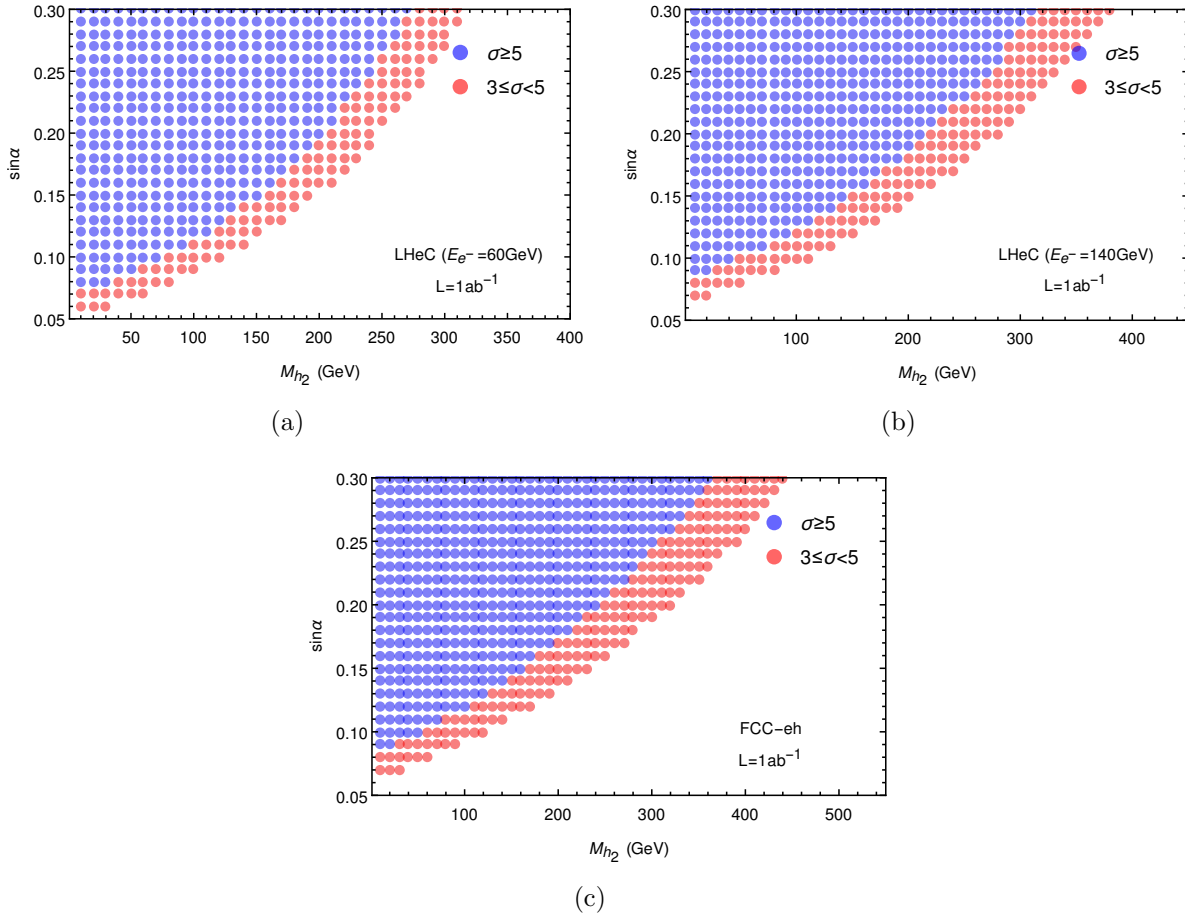


Figure 7: 3σ and 5σ detection potential regions for the signal-1 at the LHeC with $E_{e^-} = 60$ GeV (a), LHeC with $E_{e^-} = 140$ GeV (b) and FCC-eh (c) with an integrated luminosity of 1 ab $^{-1}$, respectively.

$g_{\mu\tau} = 1 \times 10^{-3}$ and the integrated luminosity being 1 ab $^{-1}$, the values of SS for signal-1 can reach 2.65 (1.84) at the LHeC with $E_{e^-} = 140$ (60) GeV and 3.42 at the FCC-eh with $E_{e^-} = 60$ GeV, $E_p = 50$ TeV. The values of SS for signal-2 can reach 8.06 (5.10) at the LHeC with $E_{e^-} = 140$ (60) GeV and 6.94 at the FCC-eh with $E_{e^-} = 60$ GeV, $E_p = 50$ TeV when we take $M_{Z_{\mu\tau}} = 0.1$ GeV, $\chi = 9 \times 10^{-5}$ GeV $^{-1}$ and an integrated luminosity of 1 ab $^{-1}$.

In Figs. 7 (a), 7 (b) and 7 (c), performing the scan over the parameter spaces of M_{h_2} and $\sin\alpha$ for $M_{Z_{\mu\tau}} = 0.1$ GeV, we show the experimental evidence region ($3 \leq \text{SS} < 5$) and experimental discovery region ($5 \leq \text{SS}$) of signal-1 at different e-p colliders with integrated luminosity being 1 ab^{-1} . For $\sin\alpha \leq 0.3$, from Fig. 7 (a), we obtain the h_2 mass region of above 3σ confidence level as $10 \text{ GeV} \leq M_{h_2} \leq 320 \text{ GeV}$ and above 5σ confidence level as $10 \text{ GeV} \leq M_{h_2} \leq 270 \text{ GeV}$ at the LHeC with $E_{e^-} = 60 \text{ GeV}$. From Fig. 7 (b), we obtain the h_2 mass region of above 3σ confidence level as $10 \text{ GeV} \leq M_{h_2} \leq 400 \text{ GeV}$ and above 5σ confidence level as $10 \text{ GeV} \leq M_{h_2} \leq 310 \text{ GeV}$ at the LHeC with $E_{e^-} = 140 \text{ GeV}$. From Fig. 7 (c), we obtain the h_2 mass region of above 3σ confidence level as $10 \text{ GeV} \leq M_{h_2} \leq 480 \text{ GeV}$ and above 5σ confidence level as $10 \text{ GeV} \leq M_{h_2} \leq 360 \text{ GeV}$ at the FCC-eh. Based on these numerical results, we can say that the possible signatures of h_2 and $Z_{\mu\tau}$ from signal-1 is limited in the lower M_{h_2} range and could be detected at e-p colliders with an integrated luminosity of 1 ab^{-1} . On the other side, the FCC-eh could offer a better detection capabilities than LHeC under the same integrated luminosity.

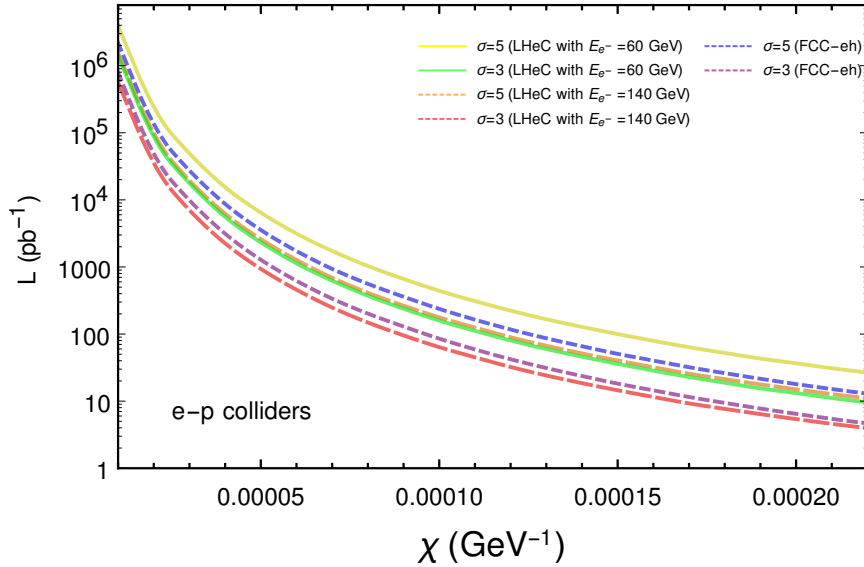


Figure 8: Integrated luminosity required for observing the signal-2 at the 3σ and 5σ statistical significance at different values of χ at e-p colliders.

The required integrated luminosities for observing the new gauge boson $Z_{\mu\tau}$ from signal-2 at the 3σ and 5σ confidence levels at different e-p colliders are plotted as functions of χ in Fig. 8. We can see that one can obtain larger statistical significance for larger χ value within allowed parameter space. We can easily obtain 5σ statistical significance for taking $\chi \geq 5 \times 10^{-5}$ within the designed luminosity region. Furthermore, the LHeC with $E_{e^-} = 140 \text{ GeV}$ has the best sensitivity to the signal-2. However, it is likely that the properties of the SM-like Higgs boson will be narrowed before 1 ab^{-1} of data are collected at an e-p collider. So we present Fig. 9 with no thought of $BR(h_1 \rightarrow \text{inv})$. In order to illustrate excluded regions of the free parameters $M_{Z_{\mu\tau}}$ and $\sin\alpha$ for reaching a given statistical significance, in Figs. 9 (a-b), we plot the 3σ and 5σ discovery of signal-2 for $g_{\mu\tau} = 1 \times 10^{-3}$ in the $\sin\alpha$ - $M_{Z_{\mu\tau}}$ plane at different e-p colliders with an integrated luminosity 1 ab^{-1} . From these figures, we can see that one can easily obtain 5σ statistical significance for taking lower values of $\sin\alpha$ in the parameter space of $M_{Z_{\mu\tau}}$. Thus, from a phenomenological point of view, the signal-2 is more likely to result in a detection of the new gauge boson $Z_{\mu\tau}$ at a lower integrated

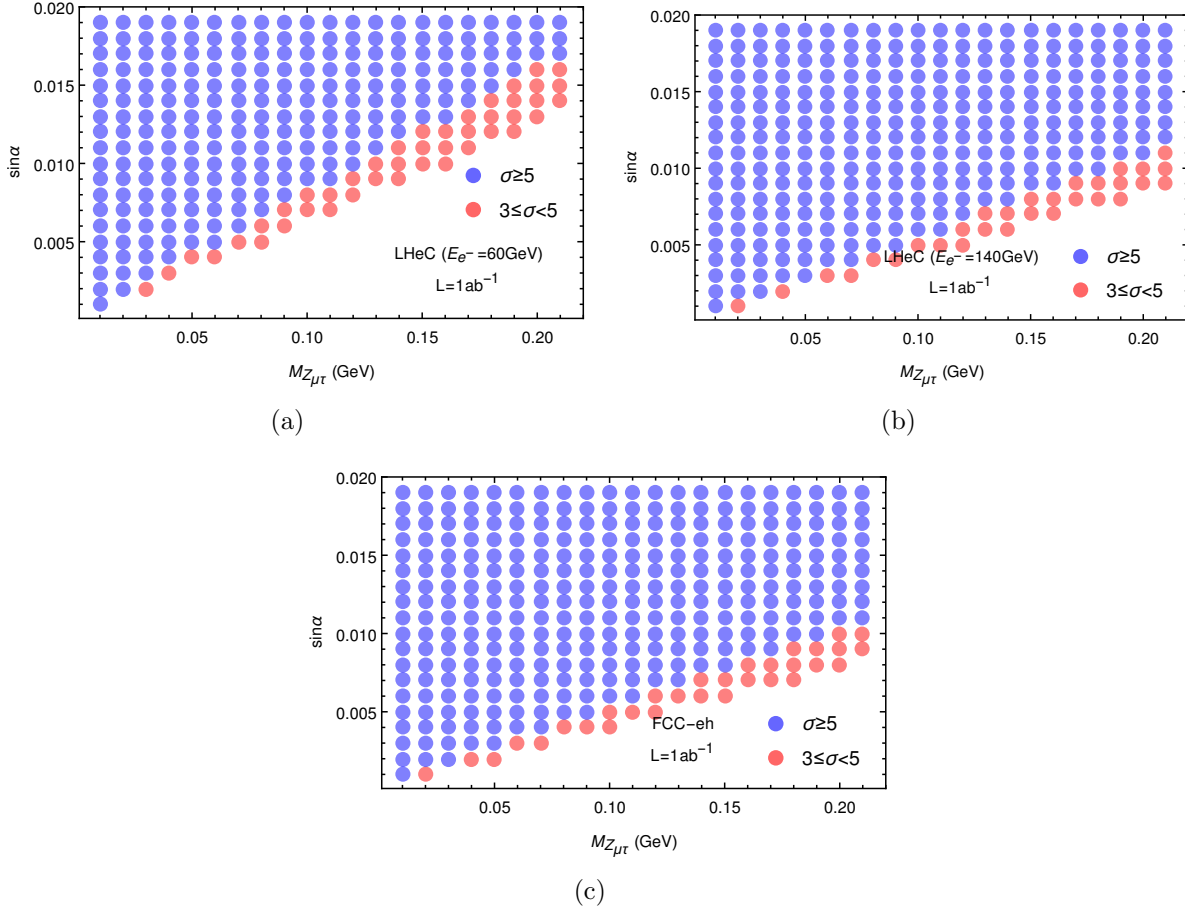


Figure 9: 3σ and 5σ detection regions for the signal-2 at the LHeC with $E_{e^-} = 60$ GeV (a), LHeC with $E_{e^-} = 140$ GeV (b) and FCC-eh (c) with an integrated luminosity of 1 ab^{-1} , respectively.

luminosity and more achievable experimental conditions.

B. $h_2 \rightarrow ZZ \rightarrow 4l$ Channel

In this subsection we proceed to investigate the prospects of e-p colliders in searching for the scalar boson h_2 by focusing on its leading decay mode ZZ

$$e^- + p \rightarrow \nu + j + h_2(\rightarrow ZZ) \rightarrow 2l^+ + 2l^- + j + \cancel{E}_T. \quad (35)$$

In above equation we have required the two Z bosons to decay leptonically, then the signal consists of two lepton pairs, one jet and a large missing transverse energy \cancel{E}_T .

For the signal $2l^+ + 2l^- + j + \cancel{E}_T$, the main sources of the irreducible backgrounds come from the processes $e^- + p \rightarrow \nu j ZZ$, $e^- j ZZ$, $e^- j W^+ W^-$, $e^- j Z W^+$, $\nu j W^+ W^-$ and $\nu j Z W^-$. Similar as above we can calculate the statistical significance easily for the luminosity of 1 ab^{-1} at e-p colliders. Our numerical results reveal that it is challenging to discover the h_2 signature through the $h_2 \rightarrow ZZ \rightarrow 4l$ channel at the e-p colliders for $M_{h_2} = 200$ (600) GeV, with $\sigma 3$ ($\sigma 5$) level statistical significance. We find that detecting this kind of signal at 3σ level requires the integrated luminosity be larger than 10^5 ab^{-1} for the benchmark point defined by $M_{h_2} = 200$ GeV, $\sin \alpha = 0.2$ and $g_{\mu\tau} = 1 \times 10^{-3}$, which extremely outreaches the designed luminosity. Thus, we do not show the relevant numerical results.

Certainly, the scalar h_2 can also decay to the modes W^+W^- , $t\bar{t}$ and h_1h_1 as long as its mass is large enough. However, the $h_2 \rightarrow WW \rightarrow \nu l 2j$ or $h_2 \rightarrow WW \rightarrow 2\nu 2l$ channel is much more difficult to reconstruct compared to the $h_2 \rightarrow ZZ \rightarrow 4l$ channel due to the final state neutrino which escapes from the detector and makes it impossible to fully reconstruct the h_2 system. So we're not going to consider the channel here even though it has a larger branching ratio than that of $h_2 \rightarrow ZZ$. We have to say that the detection of the new scalar boson h_2 via it decaying to pair of SM particles at e-p colliders is difficult to achieve at present. Of course, we also don't rule out the existence of some unique kinematic cuts that we do not take into account to optimize background suppression and improve signal observability.

VI. Conclusions

The $U(1)_{L_\mu-L_\tau}$ model, which can explain the muon $(g-2)$ anomaly, small neutrino masses and provide a candidate of DM, is phenomenologically rich and predictive. In this model, the additional scalar h_2 and gauge boson $Z_{\mu\tau}$ are obtained after spontaneous breaking of $L_\mu - L_\tau$ symmetry. New scalar h_2 mixing with the SM-like Higgs boson is helpful to improve the precision of Higgs boson measurements. Furthermore, the gauge boson $Z_{\mu\tau}$ possessing a mass around the MeV scale can explain the deficit of cosmic neutrino flux and resolve the problem of muon $(g-2)$ anomaly and relic abundance of DM simultaneously. So, studying these two new particles is of great significance for exploring this kind of new physics models. In this paper, we have studied the possibility of searching for the new particles h_2 and $Z_{\mu\tau}$ at e-p colliders. Since $Z_{\mu\tau}$ can not couple with the SM quarks and the first generation leptons, it is very difficult to be produced directly at colliders. So we consider its productions via decays of h_1 and h_2 . Although the CC production of h_1 and h_2 have larger cross sections, their final states will generate mono-jet plus missing energy, which accidentally coincides with the DIS backgrounds. Therefore we focus on NC production channels $e^-p \rightarrow e^-j h_1(\rightarrow Z_{\mu\tau} Z_{\mu\tau}) \rightarrow e^-j + \cancel{E}_T$ and $e^-p \rightarrow e^-j h_2(\rightarrow Z_{\mu\tau} Z_{\mu\tau}) \rightarrow e^-j + \cancel{E}_T$, which provide good kinematic handles to distinguish the signals from the SM backgrounds. In addition to this, we also study the CC production of h_2 and further consider its non-invisible decays(e.g. Z gauge boson) as complementary.

After giving the decay width expressions of several main decay channels of new scalar h_2 , we calculate the production cross sections of the processes $e^-p \rightarrow e^-j h_2$ and $e^-p \rightarrow \nu_e j h_2$ with the beam polarization $P(e^-) = -0.8$ in the context of the $U(1)_{L_\mu-L_\tau}$ model. The production cross sections of $Z_{\mu\tau}$ are further calculated. Then, we investigate the observability of h_2 and $Z_{\mu\tau}$ through the signal-1 from the process $e^-p \rightarrow e^-j h_2(\rightarrow Z_{\mu\tau} Z_{\mu\tau}) \rightarrow e^-j + \cancel{E}_T$ and the signal-2 from the process $e^-p \rightarrow e^-j h_1(\rightarrow Z_{\mu\tau} Z_{\mu\tau}) \rightarrow e^-j + \cancel{E}_T$ at e-p colliders with 1 ab^{-1} integrated luminosity. After simulating the signals as well as the relevant backgrounds, and applying suitable kinematic cuts on the variables \cancel{E}_T , TET, THT, $E_T(jj)$ and $E_T(e^-j)$, the values of the statistical significance SS for signal-1 can reach 2.65 (1.84) at the LHeC with $E_{e^-} = 140$ (60) GeV and 3.42 at the FCC-eh with $E_{e^-} = 60$ GeV, $E_p = 50$ TeV when we take $\sin\alpha = 0.2$, $g_{\mu\tau} = 1 \times 10^{-3}$ GeV, $M_{Z_{\mu\tau}} = 0.1$ GeV and $M_{h_2} = 300$ GeV. While for signal-2, its values can reach 8.06 (5.10) at the LHeC with $E_{e^-} = 140$ (60) GeV and 6.94 at the FCC-eh when we take $\chi = 9 \times 10^{-5}$ GeV^{-1} and $M_{Z_{\mu\tau}} = 0.1$ GeV. Performing the scan over all parameter space, we find that the signals of h_2 and $Z_{\mu\tau}$ from signal-1 is limited in the lower M_{h_2} range and could be detected at e-p colliders with an integrated

luminosity of 1 ab^{-1} . The signal of $Z_{\mu\tau}$ might be easily detected via signal-2 at e-p colliders, while the LHeC with $E_{e^-} = 140 \text{ GeV}$ has the best sensitivity to signal-2. In the end, we analysis the signals of h_2 through the CC production channel via its decaying into a pair of gauge bosons. However, due to the interference of many backgrounds and the low number of events, searching for these kind of signals are harder to achieve at e-p colliders. Thus, we expect that the possible signals of the $U(1)_{L_\mu-L_\tau}$ model might be detected at future e-p colliders via $h_2 \rightarrow Z_{\mu\tau}Z_{\mu\tau}$ and $h_1 \rightarrow Z_{\mu\tau}Z_{\mu\tau}$ channels.

ACKNOWLEDGEMENT

This work was supported in part by the National Natural Science Foundation of China under Grant Nos.11875157, 11847303 and 11605081.

References

- [1] G. Aad *et al.*, Phys. Lett. B **716**, 1 (2012).
- [2] S. Chatrchyan *et al.*, Phys. Lett. B **716**, 30 (2012).
- [3] Y. Fukuda *et al.*, Phys. Rev. Lett. **81**, 1562 (1998).
- [4] Q. R. Ahmad *et al.*, Phys. Rev. Lett. **87**, 071301 (2001).
- [5] P. A. R. Ade *et al.*, Astron. Astrophys. **571**, A16 (2014).
- [6] G. Bertone, D. Hooper and J. Silk, Phys. Rept. **405**, 279 (2005).
- [7] S. Perlmutter *et al.*, Astrophys. J. **517**, 565 (1999).
- [8] A. G. Riess *et al.*, Astron. J. **116**, 1009 (1998).
- [9] O. Cakir, A. Senol and A. T. Tasci, EPL **88**, no. 1, 11002 (2009).
- [10] H. Liang, X. G. He, W. G. Ma, S. M. Wang and R. Y. Zhang, JHEP **1009**, 023 (2010).
- [11] Z. Zhang, PoS EPS **-HEP2015**, 342 (2015).
- [12] S. Antusch, E. Cazzato and O. Fischer, Int. J. Mod. Phys. A **32**, no. 14, 1750078 (2017).
- [13] D. Curtin, K. Deshpande, O. Fischer and J. Zurita, JHEP **1807**, 024 (2018).
- [14] W. R. Porod, PoS ALPS **2018**, 024 (2018).
- [15] F. Carta, S. Giacomelli and R. Savelli, JHEP **1812**, 127 (2018).
- [16] J. Mamuzic, PoS CORFU **2017**, 060 (2018).
- [17] N. Kitazawa, JHEP **1804**, 081 (2018).
- [18] K. S. Babu and S. Jana, JHEP **1902**, 193 (2019).
- [19] T. Kon, T. Nagura, T. Ueda and K. Yagyu, arXiv:1812.09843 [hep-ph].

- [20] S. K. Kang, Z. Qian, J. Song and Y. W. Yoon, Phys. Rev. D **98**, no. 9, 095025 (2018).
- [21] P. Chaber, B. Dziewit, J. Holeczek, M. Richter, M. Zralek and S. Zajac, Phys. Rev. D **98**, no. 5, 055007 (2018).
- [22] S. P. Li, X. Q. Li and Y. D. Yang, Phys. Rev. D **99**, no. 3, 035010 (2019).
- [23] D. Azevedo, P. Ferreira, M. M. Mühlleitner, R. Santos and J. Wittbrodt, Phys. Rev. D **99**, no. 5, 055013 (2019).
- [24] K. Asai, K. Hamaguchi, N. Nagata, S. Y. Tseng and K. Tsumura, Phys. Rev. D **99**, no. 5, 055029 (2019).
- [25] B. C. Allanach, J. Davighi and S. Melville, JHEP **1902**, 082 (2019).
- [26] G. Chauhan, P. S. B. Dev, R. N. Mohapatra and Y. Zhang, JHEP **1901**, 208 (2019).
- [27] L. Delle Rose, S. Khalil, S. J. D. King, S. Moretti and A. M. Thabt, Phys. Rev. D **99**, no. 5, 055022 (2019).
- [28] A. Das, S. Goswami, V. K. N. and T. Nomura, arXiv:1905.00201 [hep-ph].
- [29] A. Das, N. Okada and N. Papapietro, Eur. Phys. J. C **77**, no. 2, 122 (2017).
- [30] A. Das, S. Oda, N. Okada and D. s. Takahashi, Phys. Rev. D **93**, no. 11, 115038 (2016).
- [31] X. G. He, G. C. Joshi, H. Lew and R. R. Volkas, Phys. Rev. D **44**, 2118 (1991).
- [32] X. G. He, G. C. Joshi, H. Lew and R. R. Volkas, Phys. Rev. D **43**, 22 (1991).
- [33] M. Drees, M. Shi and Z. Zhang, Phys. Lett. B **791**, 130 (2019).
- [34] J. X. Hou, C. X. Yue and Z. H. Zhao, Nucl. Phys. B **940**, 377 (2019).
- [35] H. Banerjee and S. Roy, Phys. Rev. D **99**, no. 3, 035035 (2019).
- [36] T. Nomura and T. Shimomura, Eur. Phys. J. C **79**, no. 7, 594 (2019).
- [37] A. Biswas, S. Choubey and S. Khan, JHEP **1702**, 123 (2017).
- [38] A. Biswas, S. Choubey and S. Khan, JHEP **1609**, 147 (2016).
- [39] E. J. Chun, A. Das, J. Kim and J. Kim, JHEP **1902**, 093 (2019).
- [40] T. Araki, S. Hoshino, T. Ota, J. Sato and T. Shimomura, Phys. Rev. D **95**, no. 5, 055006 (2017).
- [41] S. N. Gninenko and N. V. Krasnikov, Phys. Lett. B **783**, 24 (2018).
- [42] L. Delle Rose, A. Hammad and O. Fischer, arXiv:1809.04321 [hep-ph].
- [43] A. Kamada and H. B. Yu, Phys. Rev. D **92**, no. 11, 113004 (2015).
- [44] T. Araki, F. Kaneko, T. Ota, J. Sato and T. Shimomura, Phys. Rev. D **93**, no. 1, 013014 (2016).

- [45] S. Baek and P. Ko, JCAP **0910**, 011 (2009).
- [46] S. Baek, Phys. Lett. B **756**, 1 (2016).
- [47] S. Patra, S. Rao, N. Sahoo and N. Sahu, Nucl. Phys. B **917**, 317 (2017).
- [48] D. Banerjee *et al.* [NA64 Collaboration], Phys. Rev. D **97**, no. 7, 072002 (2018).
- [49] M. Anelli *et al.*, arXiv:1504.04956 [physics.ins-det].
- [50] T. Abe *et al.*, arXiv:1011.0352 [physics.ins-det].
- [51] L. Delle Rose, A. Hammad and O. Fischer, arXiv:1809.04321 [hep-ph].
- [52] F. Bordry, M. Benedikt, O. Brüning, J. Jowett, L. Rossi, D. Schulte, S. Stapnes and F. Zimmermann, arXiv:1810.13022 [physics.acc-ph].
- [53] A. Das, S. Jana, S. Mandal and S. Nandi, Phys. Rev. D **99**, no. 5, 055030 (2019).
- [54] C. Han, R. Li, R. Q. Pan and K. Wang, Phys. Rev. D **98**, no. 11, 115003 (2018).
- [55] G. Aad, et al., JHEP **1511**, 206 (2015).
- [56] Y. L. Tang, C. Zhang and S. H. Zhu, Phys. Rev. D **94**, no. 1, 011702 (2016).
- [57] T. Han and B. Mellado, Phys. Rev. D **82**, 016009 (2010).
- [58] J. Alwall *et al.*, JHEP **1407**, 079 (2014).
- [59] N. D. Christensen and C. Duhr, Comput. Phys. Commun. **180**, 1614 (2009).
- [60] R. D. Ball *et al.* [NNPDF Collaboration], Nucl. Phys. B **877**, 290 (2013).
- [61] T. Sjostrand, S. Mrenna and P. Z. Skands, JHEP **0605**, 026 (2006).
- [62] E. Conte, B. Fuks and G. Serret, Comput. Phys. Commun. **184**, 222 (2013).
- [63] M. Tanabashi *et al.*, Phys. Rev. D **98**, no. 3, 030001 (2018).